

Extracellular versus Intracellular Degradation of Nanostructured Silica Particles

Yupeng Shi, Christophe Hélyary, Bernard Haye, T. Coradin

► **To cite this version:**

Yupeng Shi, Christophe Hélyary, Bernard Haye, T. Coradin. Extracellular versus Intracellular Degradation of Nanostructured Silica Particles. *Langmuir*, American Chemical Society, 2018, 34 (1), pp.406-415. 10.1021/acs.langmuir.7b03980 . hal-01668691

HAL Id: hal-01668691

<https://hal.sorbonne-universite.fr/hal-01668691>

Submitted on 20 Dec 2017

HAL is a multi-disciplinary open access archive for the deposit and dissemination of scientific research documents, whether they are published or not. The documents may come from teaching and research institutions in France or abroad, or from public or private research centers.

L'archive ouverte pluridisciplinaire **HAL**, est destinée au dépôt et à la diffusion de documents scientifiques de niveau recherche, publiés ou non, émanant des établissements d'enseignement et de recherche français ou étrangers, des laboratoires publics ou privés.

Article

Extracellular vs. Intracellular Degradation of Nanostructured Silica Particles

Yupeng Shi, Christophe Helary, Bernard Haye, and Thibaud Coradin

Langmuir, **Just Accepted Manuscript** • DOI: 10.1021/acs.langmuir.7b03980 • Publication Date (Web): 11 Dec 2017Downloaded from <http://pubs.acs.org> on December 12, 2017**Just Accepted**

“Just Accepted” manuscripts have been peer-reviewed and accepted for publication. They are posted online prior to technical editing, formatting for publication and author proofing. The American Chemical Society provides “Just Accepted” as a free service to the research community to expedite the dissemination of scientific material as soon as possible after acceptance. “Just Accepted” manuscripts appear in full in PDF format accompanied by an HTML abstract. “Just Accepted” manuscripts have been fully peer reviewed, but should not be considered the official version of record. They are accessible to all readers and citable by the Digital Object Identifier (DOI®). “Just Accepted” is an optional service offered to authors. Therefore, the “Just Accepted” Web site may not include all articles that will be published in the journal. After a manuscript is technically edited and formatted, it will be removed from the “Just Accepted” Web site and published as an ASAP article. Note that technical editing may introduce minor changes to the manuscript text and/or graphics which could affect content, and all legal disclaimers and ethical guidelines that apply to the journal pertain. ACS cannot be held responsible for errors or consequences arising from the use of information contained in these “Just Accepted” manuscripts.



Extracellular vs. Intracellular Degradation of Nanostructured Silica Particles

Yupeng Shi, Christophe H elary, Bernard Haye and Thibaud Coradin*

Sorbonne Universit es, UPMC Univ Paris 06, CNRS, UMR 7574, Laboratoire de Chimie de la Mati re Condens e de Paris, F-75005 Paris, France

ABSTRACT: Silica nanoparticles appear as promising drug carriers for intracellular delivery. However the mechanisms by which they are degraded within cells remain largely unknown. In this context, we have prepared three types of PEGylated fluorescent silica nanoparticles with various internal structures (core-shell bio-composite, multilayered and hollow mesoporous) and studied their degradation in buffer, in culture medium and in contact with human dermal fibroblasts. All particles were prone to dissolve in solution, leading to an increase of porosity and/or precipitation of new colloids and eventually fragmentation, with a faster rate in medium compared to buffer. All particles were also uptaken by cells without significant cytotoxic effect. Their intracellular degradation occurred faster than in suspension but following almost similar dissolution mechanisms. These results strongly suggest that, in these conditions, silica nanoparticles must be primarily considered as hydrolytically degraded and not biodegraded, a point of importance for their future application in drug delivery.

INTRODUCTION

The unique features of nanomaterials have led to their rapid development in the biomedical field, for example in the delivery of drugs and genes, or for bio-imaging and diagnosis.¹⁻⁴ In this context, understanding the interactions between nanoparticles and cells is crucial to elucidate the true nature of the nanoparticle-mediated biological effects. In particular, although efforts have been devoted to discover the factors that affect the cellular uptake, toxicity and degradation of nanomaterials,⁵⁻⁸ a detailed understanding of their intracellular fate remains a true challenge.

Silica nanomaterials have been used on an industrial scale for a long time in various technological fields.⁹ They also have a variety of unique properties, such as versatile synthesis, controllable size and architecture, easy surface modification, and relatively stable and homogeneous chemical composition, which endow them with many advantages for biomedical applications.¹⁰ A number of silica-based nanomaterials with engineered shape, structure and surface modification, such as solid nanoparticles/rod, mesoporous, hollow, multilayered, core-shell nanostructure as well as bio-composite nanomaterials, have been synthesized and evaluated as drug/gene delivery systems.¹¹⁻¹⁶ However, in order to use them for intracellular delivery, successive steps of internalization, cellular trafficking, drug release and externalization should be finely controlled.¹⁷⁻¹⁹ Among these, the control of intracellular behavior of the nanoparticles remains highly challenging, especially because the question whether mammalian cells

1
2
3
4 exhibit specific biological mechanisms to degrade silica remains open.^{20,21} Indeed, the
5
6 degradation of silica nanoparticles in biologically-relevant conditions has been studied in
7
8 details and recently reviewed by Croissant *et al.*²¹ The accumulated evidences point out
9
10 the dynamic equilibrium between silica dissolution and re-deposition, which is influenced
11
12 by factors such as pH, temperature, silica concentration and porosity.²²⁻²⁵ Dove *et al.*
13
14 demonstrated that the primary dissolution event consists in the detachment of a [SiO₄]
15
16 tetrahedron from the silica surface,²⁶ that is expected to be influenced by (i) the
17
18 coordination number of Si atoms at the surface, (ii) the stability and reactivity of the
19
20 detached species and (iii) the extent of the surface and its accessibility to water.²⁷ As
21
22 reviewed by Ehrlich *et al.*,²⁸ the first two parameters are related to the condensation
23
24 degree of the silica network and the relative abundance of protonated, neutral and
25
26 deprotonated silanols while the last parameter is controlled by the specific surface area of
27
28 the system and the presence of adsorbed molecules. For instance, it has been
29
30 demonstrated that the degradation rate of silica gels with similar specific surface area
31
32 could be tuned by their condensation degree,²⁹ and that the presence of a protein coating
33
34 could slow down the dissolution process.³⁰ In parallel, Kuroda *et al.* showed that
35
36 mesoporous particles dissolve faster than plain silica particles of the same sizes.³¹ The
37
38 enhanced dissolution rate of silica particles with increasing pH and/or in the presence of
39
40 phosphate ions has also been reported at several occasions.^{21,27,28,32} Concerning the
41
42 possible redeposition of the dissolved species, a comparative study of two types of
43
44 mesoporous silica nanoparticles showed that the degradation of MCM-41-type
45
46
47
48
49
50
51
52
53
54
55
56
57
58
59
60

1
2
3
4 mesoporous silica occurred from the outer surface, while for SBA-15 nanoparticles a
5
6 decrease in microporosity and an increase in mesoporosity suggested a complex inner
7
8 solubilization/recondensation process.³³ Other studies have suggested that the
9
10 degradation of mesoporous nanoparticles may simultaneously proceed from the outer and
11
12 the inner surfaces.^{34,35}
13
14
15
16

17
18 Much less is known about the intracellular fate of silica nanoparticles. Earlier reports
19
20 on the evolution of bionanocomposite silica-biopolymer nanoparticles within the
21
22 intracellular space of mammalian cells have suggested that, after 24 h, only the
23
24 bio-organic fraction was degraded while the inorganic part remained intact.^{36,37} Further
25
26 experiments performed with mesoporous nanoparticles evidenced that their cellular
27
28 uptake was followed by their exocytosis. In addition the released particles were
29
30 associated with proteins located in the cellular membrane or involved in the vesicular
31
32 trafficking.³⁸ However no modification in particle size or morphology was reported. A
33
34 first insight in the intracellular dissolution pathway of plain silica nanoparticles was
35
36 obtained by Quignard *et al.* through a combination of TEM imaging and identification of
37
38 the products of their degradation.³⁹ A decrease of particle size was observed and
39
40 attributed to surface erosion as a result of the dissolution equilibrium of silica. Since then,
41
42 further evidences of the ability of silica to dissolve intracellularly were accumulated.⁴⁰⁻⁴³
43
44
45
46
47
48
49 Yet, considering the complexity of the accompanying trafficking events, that can include
50
51
52
53
54
55
56
57
58
59
60
61
62
63
64
65
66
67
68
69
70
71
72
73
74
75
76
77
78
79
80
81
82
83
84
85
86
87
88
89
90
91
92
93
94
95
96
97
98
99
100
101
102
103
104
105
106
107
108
109
110
111
112
113
114
115
116
117
118
119
120
121
122
123
124
125
126
127
128
129
130
131
132
133
134
135
136
137
138
139
140
141
142
143
144
145
146
147
148
149
150
151
152
153
154
155
156
157
158
159
160
161
162
163
164
165
166
167
168
169
170
171
172
173
174
175
176
177
178
179
180
181
182
183
184
185
186
187
188
189
190
191
192
193
194
195
196
197
198
199
200
201
202
203
204
205
206
207
208
209
210
211
212
213
214
215
216
217
218
219
220
221
222
223
224
225
226
227
228
229
230
231
232
233
234
235
236
237
238
239
240
241
242
243
244
245
246
247
248
249
250
251
252
253
254
255
256
257
258
259
260
261
262
263
264
265
266
267
268
269
270
271
272
273
274
275
276
277
278
279
280
281
282
283
284
285
286
287
288
289
290
291
292
293
294
295
296
297
298
299
300
301
302
303
304
305
306
307
308
309
310
311
312
313
314
315
316
317
318
319
320
321
322
323
324
325
326
327
328
329
330
331
332
333
334
335
336
337
338
339
340
341
342
343
344
345
346
347
348
349
350
351
352
353
354
355
356
357
358
359
360
361
362
363
364
365
366
367
368
369
370
371
372
373
374
375
376
377
378
379
380
381
382
383
384
385
386
387
388
389
390
391
392
393
394
395
396
397
398
399
400
401
402
403
404
405
406
407
408
409
410
411
412
413
414
415
416
417
418
419
420
421
422
423
424
425
426
427
428
429
430
431
432
433
434
435
436
437
438
439
440
441
442
443
444
445
446
447
448
449
450
451
452
453
454
455
456
457
458
459
460
461
462
463
464
465
466
467
468
469
470
471
472
473
474
475
476
477
478
479
480
481
482
483
484
485
486
487
488
489
490
491
492
493
494
495
496
497
498
499
500
501
502
503
504
505
506
507
508
509
510
511
512
513
514
515
516
517
518
519
520
521
522
523
524
525
526
527
528
529
530
531
532
533
534
535
536
537
538
539
540
541
542
543
544
545
546
547
548
549
550
551
552
553
554
555
556
557
558
559
560
561
562
563
564
565
566
567
568
569
570
571
572
573
574
575
576
577
578
579
580
581
582
583
584
585
586
587
588
589
590
591
592
593
594
595
596
597
598
599
600
601
602
603
604
605
606
607
608
609
610
611
612
613
614
615
616
617
618
619
620
621
622
623
624
625
626
627
628
629
630
631
632
633
634
635
636
637
638
639
640
641
642
643
644
645
646
647
648
649
650
651
652
653
654
655
656
657
658
659
660
661
662
663
664
665
666
667
668
669
670
671
672
673
674
675
676
677
678
679
680
681
682
683
684
685
686
687
688
689
690
691
692
693
694
695
696
697
698
699
700
701
702
703
704
705
706
707
708
709
710
711
712
713
714
715
716
717
718
719
720
721
722
723
724
725
726
727
728
729
730
731
732
733
734
735
736
737
738
739
740
741
742
743
744
745
746
747
748
749
750
751
752
753
754
755
756
757
758
759
760
761
762
763
764
765
766
767
768
769
770
771
772
773
774
775
776
777
778
779
780
781
782
783
784
785
786
787
788
789
790
791
792
793
794
795
796
797
798
799
800
801
802
803
804
805
806
807
808
809
810
811
812
813
814
815
816
817
818
819
820
821
822
823
824
825
826
827
828
829
830
831
832
833
834
835
836
837
838
839
840
841
842
843
844
845
846
847
848
849
850
851
852
853
854
855
856
857
858
859
860
861
862
863
864
865
866
867
868
869
870
871
872
873
874
875
876
877
878
879
880
881
882
883
884
885
886
887
888
889
890
891
892
893
894
895
896
897
898
899
900
901
902
903
904
905
906
907
908
909
910
911
912
913
914
915
916
917
918
919
920
921
922
923
924
925
926
927
928
929
930
931
932
933
934
935
936
937
938
939
940
941
942
943
944
945
946
947
948
949
950
951
952
953
954
955
956
957
958
959
960
961
962
963
964
965
966
967
968
969
970
971
972
973
974
975
976
977
978
979
980
981
982
983
984
985
986
987
988
989
990
991
992
993
994
995
996
997
998
999
1000

1
2
3
4 At present, there are mainly three strategies to load small molecular drugs and
5
6 biological macromolecules within silica nanomaterials. The first is to mix the drugs with
7
8 the silica precursor to form nanocomposites.^{44,45} The second is through the layer-by-layer
9
10 method.^{46,47} The third involves the impregnation of mesoporous or hollow silica
11
12 nanoparticles.^{48,49} As far as we know, there is no report comparing the degradation
13
14 behavior of these three types of silica nanoparticles in biologically-relevant conditions.
15
16
17 With this purpose, we have prepared PEGylated fluorescent silica particles with different
18
19 internal structures (bio-composite, multilayered and hollow mesoporous) and studied
20
21 their time evolution in abiotic (phosphate buffer, culture medium) conditions and then in
22
23 the presence of normal human dermal fibroblasts. Structural degradation and dissolution
24
25 kinetics of the nanoparticles were studied in parallel with their cytotoxicity. The
26
27 here-gathered data suggest that, for these systems, the intracellular fate of silica
28
29 nanoparticles can be explained on the sole basis of physico-chemical processes. This
30
31 provides new and strong evidences that, in the intracellular space, silica nanoparticles
32
33 should be considered as hydrolytically-degradable rather than biodegradable materials, a
34
35 result of great consequences for the design of silica-based biomaterials.
36
37
38
39
40
41
42
43
44
45

46 **MATERIALS AND METHODS**

47
48
49 **Chemicals.** Tetraethyl orthosilicate (TEOS), (3-Aminopropyl)triethoxysilane
50
51 (APTES), Branched polyethyleneimine (PEI, 25 kDa), Bovine serum albumin (BSA,
52
53 66 kDa), Cetyl trimethylammonium bromide (CTAB) were obtained from
54
55
56
57
58
59
60

1
2
3
4 Sigma-Aldrich. Fluorescein Isothiocyanate (Isomer I) (FITC), N-hydroxysuccinimide
5
6 (NHS) and 1-ethyl-3-(3-dimethylaminopropyl)-carbodiimide (EDC) were obtained from
7
8 Alfa Aesar. Methoxypolyethylene glycol acetic acid N-succinimidyl ester
9
10 (NHS-PEG₅₀₀₀-MAL), dimethylsulfoxide (DMSO), triethanolamine (TEA) and
11
12 ethylenediamine tetraacetic acid (EDTA) were obtained from Sigma-Aldrich. Dubelcco's
13
14 Modified Eagle Medium (DMEM) and Fetal Calf Serum (FCS) was purchased from
15
16 Gibco BRL. Unless specified, all the commercial products were used without further
17
18 purification.
19
20
21
22
23
24

25 **Synthesis of PEGylated BSA@SiO₂ Nanoparticles (BSNPs).** BSA@SiO₂
26
27 nanoparticles were synthesized via a modified Stöber method.⁵⁰ First, 30 mg BSA were
28
29 diluted in 3 mL deionized (DI) water and then added to 20 mL of ethanol containing 2
30
31 mL ammonia. After 5 minutes, 1 mL TEOS was added under stirring for 1 hour. Lastly,
32
33 50 μL APTES-FITC was added three times every two hours, followed by vigorous
34
35 stirring for 24 hours. Another 50 μL APTES was added and after for 24 hours under
36
37 stirring, amine-functionalized BSA@SiO₂-NH₂ particles were obtained, recovered by
38
39 centrifugation and washed with ethanol twice. Next, BSA@SiO₂-NH₂ were re-dispersed
40
41 in 5 mL of PBS (phosphate buffer saline, 1X), and 8 mg of NHS-PEG₅₀₀₀-MAL was
42
43 added.⁵¹ The mixture was then stirred at room temperature for 2 hours before harvesting
44
45 PEGylated particles by centrifugation.
46
47
48
49
50
51
52
53
54
55
56
57
58
59
60

Synthesis of PEGylated Hollow Mesoporous Silica Nanoparticles (HSNPs).

Fluorescent uniform ~100 nm sized SiO₂ nanoparticles were obtained using a modified Stöber method.⁵² In a typical synthesis, 35.7 mL of absolute ethanol was mixed with 5 mL water and 0.8 mL of ammonia and stirred for 5~10 minutes at room temperature. Then 1 mL of TEOS and 1 mL of APTES-FITC were added and the mixture was allowed to react at room temperature for 1 h. Afterward, SiO₂ nanoparticles were washed with water and ethanol and suspended in 20 mL of water. To prepare hollow mesoporous silica nanoparticles,⁵³ CTAB (2 g) and TEA (20 mg) were dissolved in 20 mL of DI water and stirred at room temperature for 1 h. Then, 10 mL of the previous SiO₂ suspension was added and stirred at room temperature for 1 h before addition of 0.15 mL of TEOS. The mixture was stirred for 1 h at 80°C in a water bath and the mixture was then cooled down to 50°C followed by addition of 636 mg of sodium carbonate (Na₂CO₃), under constant stirring for 30 min. To remove the CTAB, the product was extracted for 24 h with a 1 wt% solution of NaCl in methanol at room temperature. This process was carried out for at least 3 times to ensure complete removal of CTAB. For PEG grafting, 8 mg of the recovered particles were dispersed in 50 mL of DMSO and then 500 µL of APTES were added. After the mixture was stirred for 20 hours, amine-functionalized HSNPs (HSNP-NH₂) were recovered by centrifugation and washed with ethanol twice. Next, HSNP-NH₂ particles were re-dispersed in 5 mL of DMSO, and 8 mg of NHS-PEG₅₀₀₀-MAL was added. The mixture was then stirred at room temperature for 2 hours under anhydrous conditions before being harvested by centrifugation.

1
2
3
4 **Synthesis of PEGylated Double-layered PEI-Silica Nanoparticles (PSNPs).** For
5
6 the synthesis of SiO₂@PEI, 20 mL of a suspension of 100 nm FITC-doped silica
7
8 nanoparticles (*vide supra*) was added dropwise to the same volume of an aqueous
9
10 solution of PEI (10 mg.mL⁻¹).⁵⁴ After 3 additional hours of mixing, particles were
11
12 recovered by centrifugation, washed 2 times in DI water and finally re-suspended in DI
13
14 water. For the synthesis of SiO₂@PEI@SiO₂,⁴⁷ 8 mL of the SiO₂@PEI solution was
15
16 mixed with 5 mL absolute ethanol and 0.8 mL of ammonia and stirred for 10 minutes at
17
18 room temperature. Then 0.2 mL of TEOS and 20 μL APTES-FITC was added and the
19
20 mixture was allowed to react at room temperature for 16 h. Afterward,
21
22 SiO₂@PEI@SiO₂ nanoparticles were washed with water and ethanol and suspended in
23
24 20 mL of water. For the deposition of the second PEI and silica layers, the synthetic
25
26 procedure was similar to the previous one, except for the final addition of 200 μL APTES
27
28 to obtain SiO₂@PEI@SiO₂@PEI@SiO₂-NH₂ nanoparticles. Next, these particles were
29
30 re-dispersed in 5 mL of DMSO, and 8 mg of NHS-PEG₅₀₀₀-MAL was added. The
31
32 mixture was then stirred at room temperature for 2 hours under anhydrous conditions
33
34 before harvesting by centrifugation.
35
36
37
38
39
40
41
42
43
44

45 **Nanoparticle Characterization.** Particle size distribution, polydispersity index and
46
47 zeta potential (ζ) were measured in DI water or cell culture medium (DMEM) using a
48
49 ZetaSizer Nano (Malvern Instruments Ltd., Worcestershire, UK). Particles were also
50
51 imaged using Transmission Electron Microscopy (TEM) on a FEI Tecnai F₂₀ U-TWIN
52
53 electron microscope (TEM) (FEI Company, Philips, Netherlands). Dynamic Light
54
55
56
57
58
59
60

1
2
3
4 Scattering (DLS) was used to determine the hydrodynamic diameter of the nanoparticles
5
6 in Milli-Q water or in culture medium. The reading was carried out at an angle of 90° to
7
8 the incident beam (632 nm). The Contin algorithm was used to analyze the
9
10 autocorrelation functions. Fluorescence spectra of the particles suspended in water were
11
12 recorded on a Horiba Jobin Yvon fluorescence spectrometer with an excitation
13
14 wavelength of 485 nm. Nitrogen (N₂) sorption measurements were performed at 77K
15
16 using an accelerated surface area and porosimetry analyzer with Brunauer-Emmett-Teller
17
18 (BET) calculations for the surface area.
19
20
21
22
23

24 **Dissolution and Degradation Assays in Buffer and Culture Medium.** To carry
25
26 out the *in vitro* degradation experiments in abiotic conditions, a suspension of each type
27
28 of PEGylated particles at a 0.4 mg.mL⁻¹ concentration was left under mild stirring at
29
30 37°C in phosphate buffer saline (PBS) 1X or DMEM. The fluorescence intensity of the
31
32 medium was analyzed at selected time intervals after centrifugation in a Nanosep® 3kD
33
34 centrifugal device to separate particles, that were further used for TEM observation, and
35
36 solutions to monitor the proportion of released silane-FITC over time.³⁹ All experiments
37
38 were performed in triplicate.
39
40
41
42
43
44

45 **Cells and Treatments with Nanoparticles.** Normal human dermal fibroblasts
46
47 (from Promocell) were grown in DMEM supplemented with FCS (10%), penicillin (100
48
49 units.mL⁻¹), streptomycin (100 mg.mL⁻¹, from Gibco BRL) and fungizone (0.25 mg.mL⁻¹,
50
51 from Gibco BRL). The culture flasks (75 cm²) were kept at 37 °C in 95% humidity and
52
53 5% CO₂ atmosphere. At confluence, fibroblasts were removed from cultured flasks by
54
55
56
57
58
59
60

1
2
3
4 treatment with 0.1% trypsin and 0.02% EDTA. Cells were rinsed, centrifuged and
5
6 dispersed in the supplemented DMEM medium. Fibroblasts were used at passage 8 for
7
8 the experiments.
9

10
11
12 **Nanoparticle Internalization, Degradation and Release.** The cells were seeded
13
14 at a density of 30,000 cells per well in 24-well plate with round glass coverslips at the
15
16 bottom of the wells and kept 24 h with culture medium at 37 °C in 95% humidity and 5%
17
18 CO₂ atmosphere previous to incubation with 0.4 mg.mL⁻¹ of the three types of silica
19
20 nanoparticles. For fluorescence microscopy, cells were collected at day 1, 2 and 7,
21
22 washed three times with PBS 1X, and fixed with 4% paraformaldehyde in PBS (1 h, 4
23
24 °C). Staining of the nuclei with DAPI (Invitrogen) was perform via incubation for 15 min
25
26 at room temperature and rinsing with HBSS 1X before observation with a fluorescent
27
28 microscope (Axio 100, Carl Zeiss). For TEM, cells were fixed at day 1, 2 and 7 using
29
30 3.63% glutaraldehyde in a 0.05 M sodium cacodylate buffer with 0.3 M saccharose for 1
31
32 h at 4 °C. Samples were washed three times before post-fixing with 2% osmium
33
34 tetraoxide for 1 h at 4 °C. Cells were then detached from the culture flasks by scratching
35
36 and centrifuged. The pellets were embedded in a 4 mg.mL⁻¹ collagen hydrogel to ease
37
38 sectioning and cellular observations. With this purpose, 50 µL of the type I collagen
39
40 solution (in 17 mM acetic acid) was neutralized by 5 µL of PBS and mixed with the
41
42 pellet. Mixtures were left for 30 minutes at 20°C to allow collagen gelation. Recovered
43
44 hydrogels were fixed with 4% paraformaldehyde in PBS (1 h, 4 °C). Last, cell-containing
45
46 collagen hydrogels were dehydrated with an ascending ethanol series ending with
47
48
49
50
51
52
53
54
55
56
57
58
59
60

1
2
3
4 propylene oxide and embedded in araldite. Ultrathin sections were prepared with an
5
6 Ultracut ultramicrotome (Leica, France). Slides were analyzed with a JEOL 1011
7
8 electron microscope operating at 120 kV. Images were obtained for at least 10 cells for
9
10 each sample.
11
12

13
14
15 To follow the kinetics of particles degradation and release, continuous cultures were
16
17 first performed over 1 week in the presence of $0.4 \text{ mg}\cdot\text{mL}^{-1}$ silica nanoparticles. After this
18
19 delay, the culture medium was removed and cells were rinsed before adding fresh
20
21 medium and performing an additional incubation period of 7 days. Fluorescence and
22
23 TEM imaging, as well as fluorescence measurements of the whole medium and of its
24
25 soluble content were performed as described above. All experiments were performed in
26
27 triplicate.
28
29
30
31

32
33
34 **Toxicological Assays.** Cellular metabolic activity of cells in 24-well plate after 2
35
36 days of contact with silica particles at concentrations $0.025\text{-}0.400 \text{ mg}\cdot\text{mL}^{-1}$ and after 1, 2,
37
38 7 and 14 days of incubation with $0.4 \text{ mg}\cdot\text{mL}^{-1}$ silica nanoparticles was evaluated using
39
40 Alamar Blue assay (n=6). After incubation, cells were rinsed with medium and incubated
41
42 at $37 \text{ }^\circ\text{C}$ in a humidified 5% CO_2 air atmosphere for 4 h with a 10% solution of Alamar
43
44 blue in phenol red-free culture medium. Absorbance of the medium at 570 nm and 600
45
46 nm was recorded with a UV-visible spectrophotometer and the percentage of dye
47
48 reduction was calculated. The results were expressed as a percentage of viability assessed
49
50
51
52
53
54
55
56
57
58
59
60

1
2
3
4 in control samples (incubated with no nanoparticles). It is worth mentioning that
5
6 incubation of the particles alone with Alamar Blue gave negligible absorbance values.
7
8

9
10 **Statistical Analysis.** Statistical significance of differences was evaluated by a
11
12 Wilcoxon-MannWhitney test. This test was chosen instead of Student t test according to
13
14 the result of Shapiro-Wilk normality test. A value of $P < 0.05$ was considered significant.
15
16
17
18
19

20 21 22 **RESULTS AND DISCUSSION**

23
24
25
26

27 **Synthesis and Functionalization of Nanostructured Silica Particles.** Silica
28
29 nanoparticles with different internal structures were synthesized and characterized using
30
31 transmission electron microscopy (TEM), dynamic light scattering (DLS) and zeta
32
33 potential measurements. PEGylated BSA-coated silica nanoparticles, PEI-coated silica
34
35 nanoparticles and hollow mesoporous silica nanoparticles were named as BSNPs, PSNPs
36
37 and HSNPs respectively.
38
39
40
41

42
43 Fairly uniform BSNPs were prepared by using a modified Stöber method in the
44
45 presence of BSA. As shown in the TEM images (**Figure 1a,d**), the BSNPs are spherical in
46
47 shape with a mean diameter of ~45 nm. They exhibit a well-contrasted core-shell structure
48
49 suggesting that they consist of a silica-rich layer coating a BSA-rich internal domain.⁵⁰
50
51
52
53
54
55
56
57
58
59
60

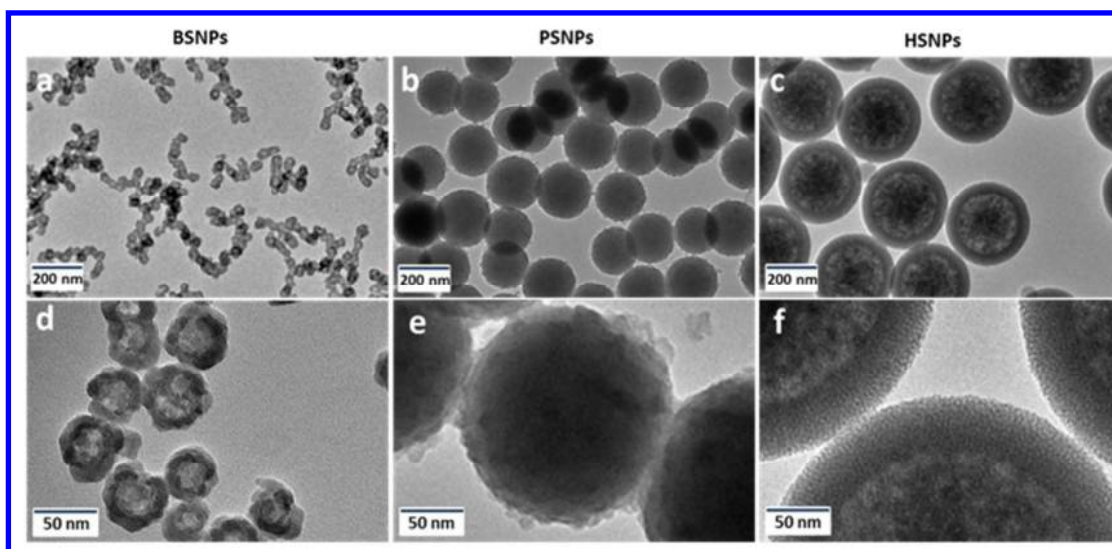


Figure 1 : TEM images of the as-prepared PEGylated fluorescent silica nanoparticles: (a, d) BSNPs; (b, e) PSNPs and (e, f) HSNPs.

Table 1 : Mean diameter D_m from DLS and TEM, Zeta potential ζ in deionized water and culture medium.

	D_m DLS	D_m TEM	ζ water	ζ medium
	(nm)	(nm)	(mV)	(mV)
BSNPs	109 ± 6	44 ± 2	-15 ± 1	-8 ± 1
PSNPs	190 ± 6	176 ± 4	-8 ± 1	-5 ± 1
HSNPs	310 ± 10	261 ± 7	-11 ± 1	-7 ± 1

DLS measurements in deionized water indicated a two-fold increase in the mean diameter D_m , compared to TEM, suggesting that some aggregation occurred, although to a limited

1
2
3
4 extent (**Table 1** and **Figure S1**). This aggregation was confirmed by performing a DLS
5
6 analysis of a BSNPs suspension just after sonication, yielding to a D_m value of 44 ± 10
7
8 nm (**Figure S1**). The successful functionalization process with amine and then PEG
9
10 groups was evidenced by size and ζ potential modifications (**Table S1** in ESI): whereas
11
12 the as-prepared BSA@SiO₂ exhibited a strongly negative ζ value, APTES grafting led to
13
14 a slightly positive ζ value due to ammonium groups. This was correlated with an
15
16 increase in the D_m value as obtained by DLS, in agreement with the decrease of
17
18 ζ absolute value leading to a lower colloidal stability. After PEG grafting, the D_m value
19
20 obtained by DLS decreased, due to the ability of the polymer coating to limit BSNPs
21
22 aggregation, and the ζ value became negative, due to the reaction of some of the surface
23
24 amine groups with NHS-PEG₅₀₀₀-MAL.
25
26
27
28
29
30
31
32

33 PSNPs were obtained from plain silica nanoparticles by a layer-by-layer method
34
35 using branched PEI (25 kDa). Starting from ~100 nm Stöber nanoparticles, two
36
37 successive sequences of PEI deposition/silica coating were performed. Variations in
38
39 ζ value occurred as expected, *i.e.* $\zeta > 0$ for outer PEI layer and $\zeta < 0$ after silica
40
41 deposition (**Table S1** in ESI). Again, APTES grafting turned the particle surface positive
42
43 while PEG conjugation ultimately led to negatively-charged PSNPs in deionized water
44
45 (**Table 1**). The accompanying modifications of hydrodynamic diameter, as obtained by
46
47 DLS, are difficult to analyze in details in terms of size variations as they are the result of
48
49 PEI conformation on the particle surface, silica layer thickness as well of the aggregation
50
51 tendency of the different systems. Nevertheless TEM imaging (**Figure 1b**) provides a D_m
52
53
54
55
56
57
58
59
60

1
2
3
4 value of ~ 175 nm and therefore an overall coating thickness of ~ 35 nm, clearly
5
6 evidenced at higher magnification (**Figure 1e**).

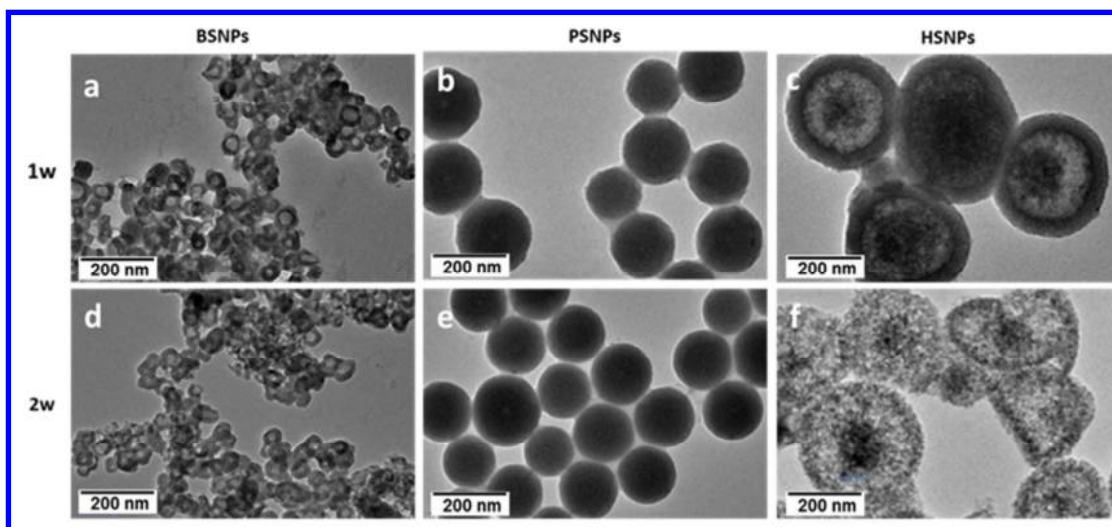
7
8
9
10 Hollow HSNPs were prepared by etching 100 nm-Stöber nanoparticles following the
11
12 method proposed by Chen et al.⁵³ TEM imaging clearly showed that HSNPs have a
13
14 spherical morphology and uniform particle size ~ 260 nm, with a porous shell thickness
15
16 of ~ 50 nm and a highly porous core, although a central denser region, corresponding to
17
18 unreacted part of the starting Stöber particles, could sometimes be distinguished (**Figure**
19
20 **1c,f**). The overall synthetic process was also followed by DLS and ζ -metry (**Table S1**),
21
22 showing that despite the fact that APTES-modified intermediates are particularly prone to
23
24 aggregation ($D_m = 780 \pm 40$ nm), the PEG coating efficiently enhances the colloidal
25
26 stability of final HSNPs particles ($D_m = 310 \pm 10$ nm in deionized water compared to 260
27
28 ± 7 nm from TEM) (**Table 1**). Nitrogen adsorption-desorption isotherm measurements
29
30 indicated that the HSNPs had a relatively high specific surface area of *ca.* $550 \text{ m}^2 \cdot \text{g}^{-1}$ and
31
32 a well-defined mean pore size of 3.9 nm (**Figure S2**).

33
34
35
36
37
38
39
40
41
42 Altogether, when the three types of particles are compared, their size, as obtained
43
44 from both DLS in deionized water and TEM, vary in the order HSNPs > PSNPs >
45
46 BSNPs. In terms of surface properties, their zeta potential in deionized water (pH 6.5) is
47
48 always negative and follows the PSNPs > HSNPs > BSNPs evolution. Interestingly, the
49
50 same order of ζ values is found for NH_2 -grafted particles, suggesting that the PEG
51
52 coupling occurred in a similar extent for the three systems. This order is preserved over
53
54
55
56
57
58
59
60

1
2
3
4 the whole pH 2-11 range with apparent isoelectric points (IEP) of ca. 4.5, 5.5 and 6.2 for
5
6 BSNPs, HSNPs and PSNPs, respectively (**Figure S3**). It is also maintained in cell culture
7
8 medium although with some minor variations between the different particles. A
9
10 systematic increase in ζ values compared to deionized water is observed that very likely
11
12 indicates the surface adsorption of positively-charged proteins present in FCS-enriched
13
14 DMEM (**Table 1**).⁵⁵ The incorporation of FITC within the different nanoparticles was
15
16 checked by fluorescence measurements. As shown in **Figure S4**, the FITC-doped silica
17
18 nanoparticles gave rise to a strong emission, with no significant shift in the maximum
19
20 wavelength compared to the dye alone. However, at a constant particle concentration, the
21
22 signal intensity varied from one particle type to the other. Such a difference may reflect
23
24 various silica contents in the nanoparticle structures. For instance, the lowest intensity
25
26 was obtained for BSNPs, *i.e.* hybrid nanoparticles containing large amounts of BSA.
27
28 However, other processes such as FITC fluorescence variations due to different dye
29
30 environment and mobility may also contribute to these differences.⁵⁶
31
32
33
34
35
36
37
38
39
40

41 **Behaviour of Nanoparticles in Buffer and Cell Culture Medium.** To investigate
42
43 the influence of the internal structure of silica nanoparticles on their degradation in
44
45 abiotic (*i.e.* cell-free) media, TEM imaging and monitoring of the kinetics of silica
46
47 dissolution was first performed in a PBS buffer (pH 7.4) at 37 °C over 2 weeks. After one
48
49 week, all nanoparticles showed a clear tendency to form aggregates under TEM imaging
50
51 conditions (**Figure 2**). For BSNPs, the core-shell structure is overall preserved but some
52
53 particles appear to have grown in size and the contrast between the inside and outside
54
55
56
57
58
59
60

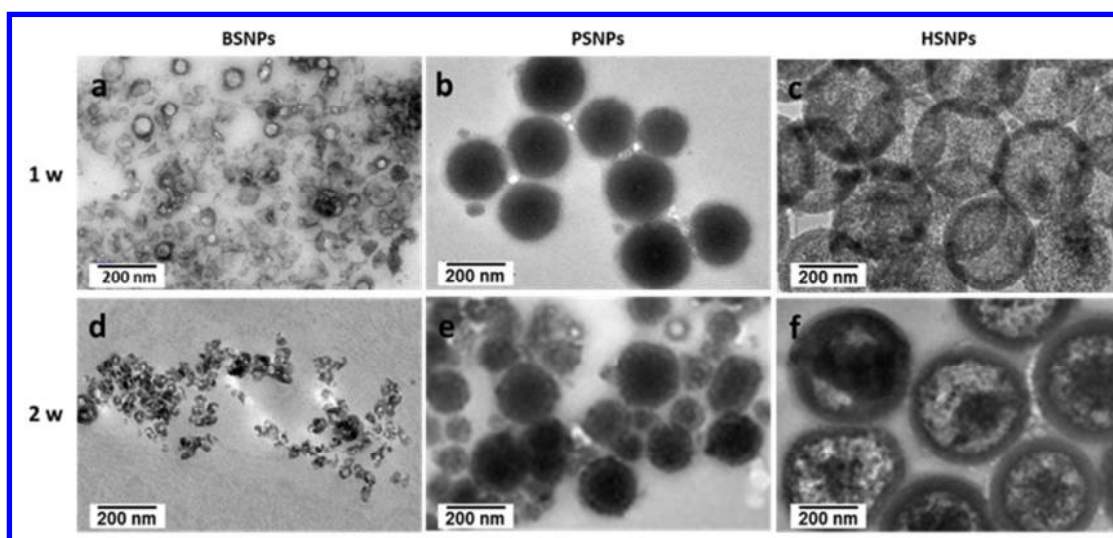
1
2
3
4 parts has increased compared to the initial particles. For PSNPs, the outer silica shell is
5
6 less well-defined. No further evolution could be evidenced for these two sets of particles
7
8 after one additional week, except for a higher tendency to aggregate. In parallel, the
9
10 internal structure of HSNPs does not appear much modified after one week but some
11
12 deformed particles are observed. After two weeks, they have turned into highly porous
13
14 particles with a weaker contrast between the shell and the core parts, some of them being
15
16 particles with a weaker contrast between the shell and the core parts, some of them being
17
18 obviously fractured.
19
20
21



39
40
41 **Figure 2:** TEM imaging of the structural evolution of silica nanoparticles in PBS after
42 (a-c) one and (d-f) two weeks.
43
44
45

46
47 The dissolution of these different particles was also studied in the DMEM cell
48
49 culture medium at 37 °C (**Figure 3** and **Figure S5** for higher magnification images). For
50
51 BSNPs, after one week, some particles have grown in size while others are broken. Only
52
53 small fragments could be recovered after 2 weeks. For PSNP samples after 1 week, the
54
55
56
57
58
59
60

1
2
3
4 outer coating has a shallow appearance and is decorated with porous particles 10-30 nm
5
6 in diameter. Strikingly, after two weeks, two populations of particles are observed: larger
7
8 ones, *ca.* 100-150 nm in diameter, exhibiting a dense core and a porous shell, and smaller
9
10 ones, 20-50 nm in size, with a porous internal structure resembling that of
11
12 previously-observed decorating particles. Such an evolution would suggest dissolution of
13
14 the silica material constituting PSNPs shell and core and its reprecipitation into smaller
15
16 particles. To support this hypothesis, a more detailed analysis by TEM of the kinetics of
17
18 degradation of these nanoparticles was performed, evidencing that the progressive
19
20 appearance of the porous external small particles was correlated with a decrease in the
21
22 density of the largest ones (Figure S6)

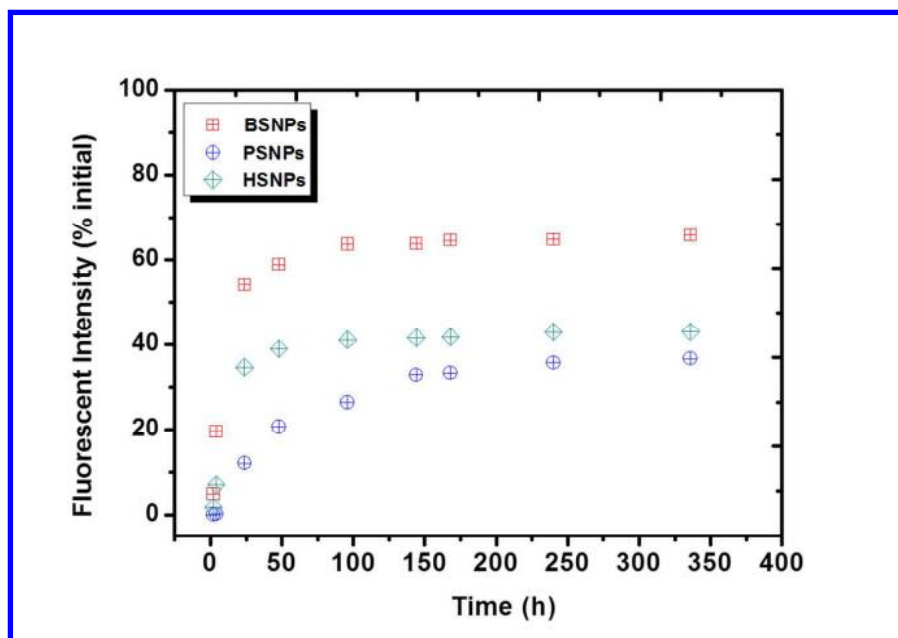


30
31
32
33
34
35
36
37
38
39
40
41
42
43
44
45
46
47 **Figure 3** : TEM imaging of the structural evolution of silica nanoparticles in DMEM
48 culture medium after (a-c) on week and (d-f) two weeks.

49
50
51
52
53 For HSNPs, TEM images after 1 week are highly reminiscent of those previously
54
55 obtained in PBS after 2 weeks. Within two weeks, after centrifugation and washing, only
56
57

1
2
3
4 a few of these nanoparticles could be recovered with an intact morphology and imaged.
5
6 These particles seem to have grown in size and the shell and core particle appear denser
7
8 and separated by a highly porous, if not empty, region. Hence, overall, the culture
9
10 medium appears to speed up the degradation process of all particles compared to PBS at a
11
12 similar pH.
13
14
15

16
17
18 In parallel, the dissolution rate of the particles in culture medium was investigated
19
20 through the monitoring of the fluorescence of the solution after centrifugation and
21
22 filtration. Because these steps eliminate silica particles and since FITC forms a stable
23
24 covalent bond with the silica network, the fluorescence signal can only correspond to
25
26 FITC-silane or soluble FITC-polysiloxane molecules released upon silica dissolution.³⁹
27
28
29
30



1
2
3
4 **Figure 4** : Evolution of the content of the culture medium over 2 weeks in the presence
5
6 of silica nanoparticles as monitored by the fluorescence intensity of FITC-labelled
7
8 soluble forms of silica.
9

10
11
12 After 1 day, more than 50 % of the BSNPs particles are dissolved and the maximum
13
14 dissolution of 65 % is reached after 1 week (**Figure 4**). For HSNPs, a similar rapid
15
16 dissolution is observed but the maximum dissolution of 40 % is reached after 1 week.
17
18 PNSPs dissolve much more slowly (*ca.* 10 % after 1 day) and, after 2 weeks, only 30 %
19
20 of the initial fluorescent silanes are present in a soluble form. These data confirm the low
21
22 stability of BSNPs in DMEM. For PNSPs, the low degradation rate and extent are in
23
24 favor of the proposed mechanism of progressive reprecipitation of the soluble forms
25
26 originating from the shell and then core particle dissolution. HSNPs represent an
27
28 intermediate case, with fast initial dissolution rate followed by a plateau and low
29
30 dissolution extent, suggesting that some reprecipitation reactions also occur, but in a less
31
32 efficient manner than in PNSPs
33
34
35
36
37
38
39
40
41

42 **Nanoparticles Behaviour in the Presence of Fibroblasts.** To study the possible
43
44 impact of nanoparticle structure and degradation on cell viability, NHDF cells were used
45
46 as model organisms and the Alamar Blue method, which measures the mitochondrial
47
48 activity of the cells, was selected to monitor the cellular response to nanoparticles
49
50 (**Figure 5**). After a 48 h incubation period, in all the range of concentrations tested,
51
52 BSNPs and HSNPs did not show a significant toxicity while PNSPs induced an initial
53
54
55
56
57
58
59
60

slight reduction of cell viability in all conditions, down to 75% of cell viability at a 400 $\mu\text{g}\cdot\text{mL}^{-1}$ dose. However, at this concentration, NHDFs recovered from PSNPs cytotoxicity after 1 week.

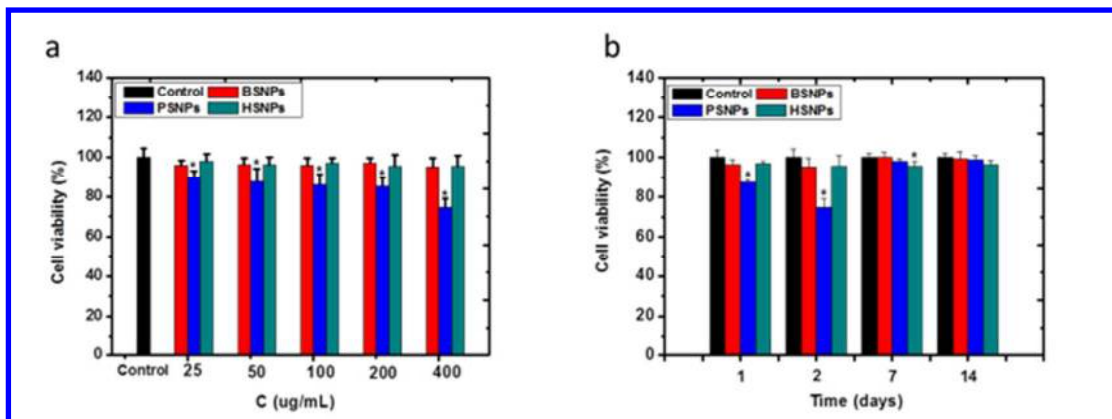
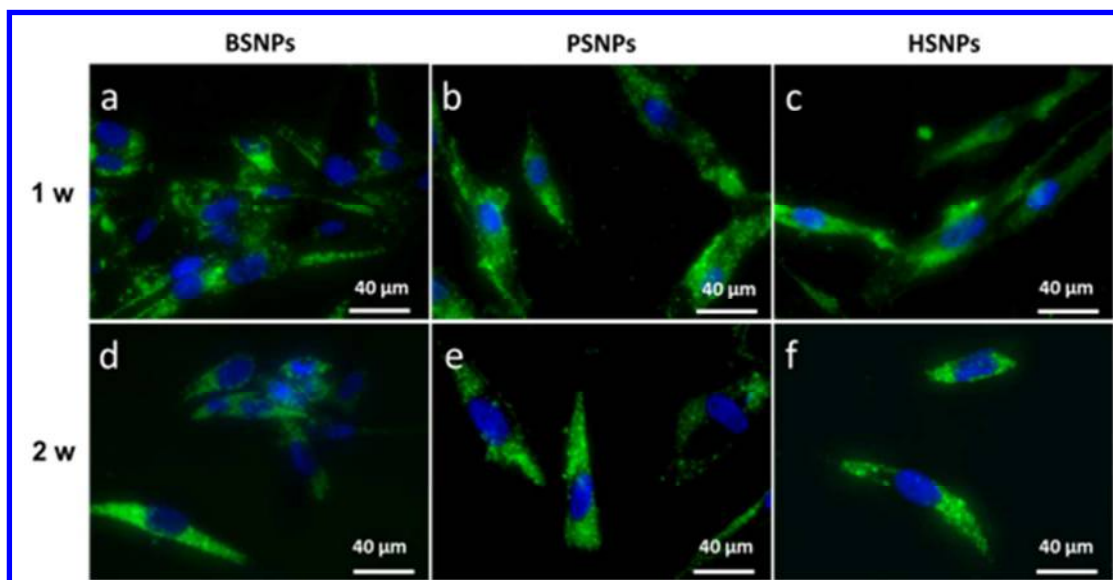


Figure 5: (a) Alamar blue assay results for NHDF cells after incubation with silica nanoparticles at various concentrations (25-400 $\mu\text{g}\cdot\text{mL}^{-1}$) for 2 days. (b) Alamar blue assay results for NHDF cells after incubation with 400 $\mu\text{g}\cdot\text{mL}^{-1}$ of silica nanoparticles at various time intervals (1-14 days). The data represent six separate experiments. Mean values \pm SD. * $P < 0.05$ versus a control group.

Referring to the dissolution kinetics shown in **Figure 4**, neither BNSPs nor their degradation products have significant cytotoxic effects. PSNPs are cytotoxic on the short term, a period where the outer layers are slowly dissolving. This result can be correlated to previous reports showing that the presence of an external silica layer decreases the toxicity of poly-lysine-coated gold nanoparticles.⁵⁷ On this basis, it can be suggested that the initial dissolution of the silica layers leads to the release of cytotoxic PEI. However,

1
2
3
4 the redeposition of smaller silica particles on PNSPs surface, as observed in **Figure 3**,
5
6 may circumvent this effect on the longer term.
7
8
9

10 The particle uptake by NHDFs in culture medium was followed by fluorescent
11 microscopy using the same silica concentration ($400 \mu\text{g}\cdot\text{mL}^{-1}$). After 24 h, silica
12 nanoparticles associated with cells were evidenced but many of them appeared to be
13 attached to the cell membrane as aggregates (**Figure S7**). With time, these aggregates
14 became less visible and the fluorescent signal appeared confined within the cell interior,
15 with a higher intensity for PSNPs and HSNPs compared to BSNPs after 2 weeks (**Figure**
16
17
18
19
20
21
22
23
24
25
26 **6**).
27
28
29
30
31
32
33



1
2
3
4 **Figure 6:** Fluorescence optical imaging of human dermal fibroblast cells after (a-c) 7
5
6 days and (d-f) 14 days of contact with $400 \mu\text{g}\cdot\text{mL}^{-1}$ silica nanoparticles. DAPI was used
7
8 for blue staining of the nucleus and green fluorescence corresponds to FITC. (Scale bar =
9
10
11
12 40 μm).
13
14
15
16
17

18
19 However, to fully ascertain particle internalization, TEM imaging was performed
20
21 (**Figure 7** and **Figure S8** for lower magnification images). After 1 week, BSNPs are
22
23 sparingly found as intracellular aggregates of particles that have decreased in size as an
24
25 apparent consequence of shrinking after core material removal. PSNPSs and HSNPs are
26
27 more easily distinguished both outside and inside the cells. The former appear as plain
28
29 particles decorated with smaller particles. For HSNPs the shell has grown in thickness
30
31
32 while the internal structure has started to degrade, as previously observed in DMEM after
33
34
35
36
37 2 weeks.
38
39
40
41
42
43
44
45
46
47
48
49
50
51
52
53
54
55
56
57
58
59
60

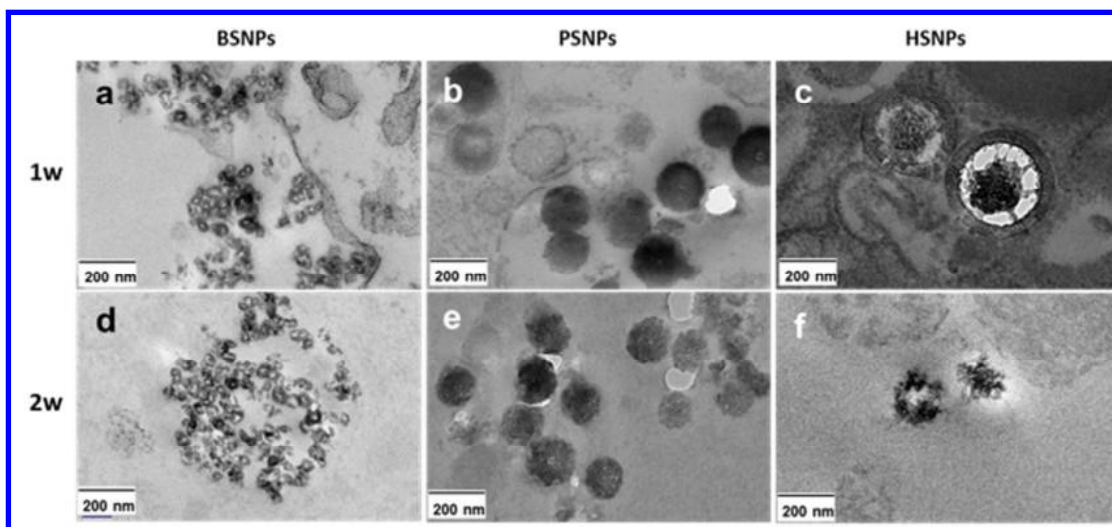
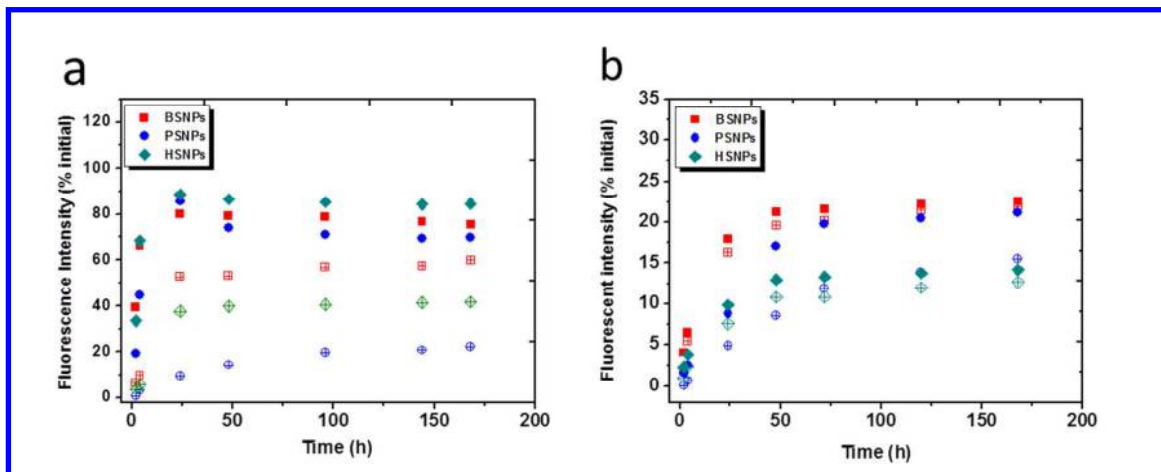


Figure 7 : TEM images of NHDF cells after (a-c) 1 week and (d-f) 2 weeks of contact with $400 \mu\text{g.mL}^{-1}$ silica nanoparticles.

Degradation and Release Kinetics. The kinetics of degradation and release of the nanoparticles was further studied by keeping NHDFs in contact with silica nanoparticles for 1 week after which the cells were rinsed off the remaining external particles and incubated in fresh culture medium for an additional week. Over the first 24 h, for all particles, the total fluorescence of the solution is initially very low and then increase progressively up to *ca.* 80 % of the intensity of the initial particle suspension (**Figure 8a**). This can be correlated with fluorescence optical imaging indicating that particles first adhere on the cell surface (decreasing the amount of free particles in solution) and are then progressively detached. Yet a decrease in total fluorescence intensity is observed after 48 h, that may reflect enhanced particle internalization.³⁹ Considering the release of soluble forms in the culture medium, the kinetics profiles are very similar to those obtained in the absence of NHDF. However, the maximum apparent dissolution ratio is

1
2
3
4 significantly smaller for BSNPs (50 % compared to 60 % without NHDF) and PSNPs (20
5
6 % compared to 30 %). This would suggest that a fraction of the soluble forms is retained
7
8
9 by the cells.
10



27
28
29 **Figure 8:** Evolution of the content of the NHDF cells culture medium as monitored by
30 the fluorescence intensity of FITC-labelled condensed and soluble forms of silica (filled
31 symbols) and soluble forms only (open symbols) (a) over 1 week in the presence of silica
32 nanoparticles and (b) over 1 additional week in a fresh medium.
33
34
35
36
37
38
39

40 After cell rinsing and incubation in a fresh, particle-free medium for an additional
41 week, intracellular nanoparticles were more difficult to observe in TEM imaging fields
42
43 (Figure 7d and Figure S8). When this was possible, we did not evidence any clear
44
45 change for BSNPs compared to day 7. PSNPs have significantly decreased in size and
46
47 exhibit a porous structure. No well-defined HSNPs could be observed after this period
48
49 and only fragments could be imaged that may originate from their full dissociation. In
50
51 parallel, the total FITC fluorescence intensity in the culture medium, initially equal to
52
53
54
55
56
57
58
59
60

1
2
3
4 zero because of the incubation in a fresh medium, increased with time (**Figure 8b**). At
5
6 the end of this additional period, almost all the initial fluorescence intensity (as calculated
7
8 by adding 1 week values obtained from Figure 8a and 2 weeks values from Figure 8b)
9
10 was recovered for the three kinds of particles, indicating that a negligible fraction of
11
12 silica remains inside the cells, in agreement with TEM experiments. However, whereas
13
14 BSNPs and HSNPs were almost fully released in a soluble form, more than 30 % of
15
16 PSNPs were externalized in a colloidal form.
17
18
19
20
21
22

23 **Degradation Pathways.** BSNPs initially show TEM-contrasting internal features
24
25 that suggest that they consist of a protein-rich interior surrounded by a silica-rich coating.
26
27 In PBS, these particles grow in size, with an apparent leakage of the core material, the
28
29 process being accelerated in culture medium. Finally, particle degradation occurs, leaving
30
31 much smaller empty particles. A similar process seems to occur within the NHDF cells,
32
33 although at a higher rate. Additional experiments performed using BSNPs incorporating
34
35 FITC-labelled BSA showed that, after one week of contact with NHDF, the protein was
36
37 hardly detectable within or at the vicinity of the cells whereas silica was still present in
38
39 large amounts (compare **Figure S9** with **Figure 6a**). The most likely explanation of these
40
41 evolutions is that water penetration within the particle leads to the swelling of the BSA
42
43 core, disruption of the silica shell and leakage of the protein (**Figure 9**). As suggested
44
45 earlier, the enzymatic degradation of BSA in the intracellular compartment may
46
47 contribute to accelerate these processes.
48
49
50
51
52
53
54
55
56
57
58
59
60

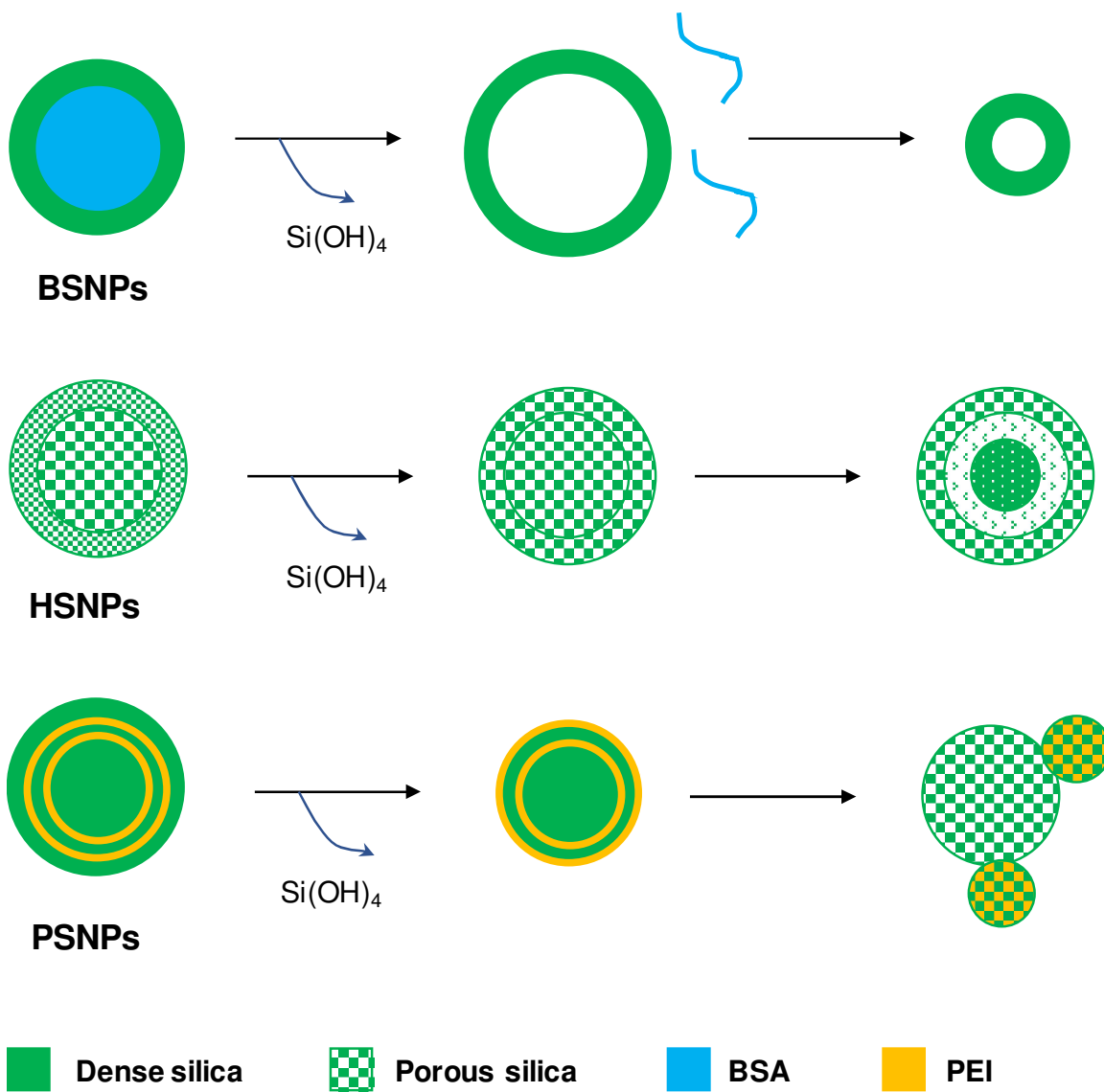


Figure 9: Schematic representation of the degradation pathways of BSNPs, HSNPs and PSNPs in DMEM culture medium.

For HSNPs, silica dissolution in PBS apparently occurs first from the shell, resulting in particles that are almost uniformly porous except for the central part and are prone to

1
2
3
4 deformation and breaking (**Figure 9**). The same process occurs in culture medium but
5
6 after two weeks, the only remaining particles exhibit a highly contrasted shell and a
7
8 denser central part, separated by a nearly empty corona. Such structures were also
9
10 observed after one week within cells and evolved towards a complete disintegration after
11
12 2 weeks. While the initial shell dissolution should be favored by its mesoporous structure,
13
14 the following process can be explained considering the dissolution of the more porous
15
16 (*i.e.* more soluble) silica corona located between the shell and the core particle and its
17
18 reprecipitation on these two denser (*i.e.* less soluble) regions, based on the Ostwald
19
20 ripening principle.
21
22
23
24
25
26
27

28 Overall BSNPs and HSNPs evolve more rapidly but along similar pathways in PBS,
29
30 in DMEM and in the intracellular space. When experiments in buffer and culture medium
31
32 are compared, pH and total silica concentration are similar. Ionic strength of DMEM is
33
34 0.13 M, being therefore comparable with the 0.16 M value for PBS 1X. However,
35
36 DMEM supplemented with FCS contains several bio-organic components (amino acids,
37
38 proteins) that can interact with silica. For instance, it was shown that histidine and
39
40 phenylalanine could promote silica dissolution.²⁸ Extending this discussion to
41
42 intracellular compartments is indeed difficult as their composition is complex and
43
44 variable. Nevertheless it is worth pointing out that lysosomes were reported to contain a
45
46 high fraction of free amino acids.⁵⁸ It is also interesting to note that intracellular
47
48 compartments that are involved in nanoparticle trafficking are reported to be slightly
49
50 (endosomes) to significantly (lysosomes) acidic so that a decrease of silica dissolution
51
52
53
54
55
56
57
58

60

1
2
3
4 rate could be expected compared to neutral conditions of PBS/DMEM medium. While
5
6 this point would require a detailed investigation of the particle structural modification in
7
8 the first hours of the internalization process, our experiments suggest that the difference
9
10 in pH conditions is not of primary importance for their long-term fate.
11
12
13

14
15 However, another important point must be taken into consideration. The full release
16
17 of silicon species from the cells to the medium clearly demonstrates that the products of
18
19 the intracellular dissolution reaction can be externalized in a continuous manner. Hence,
20
21 whereas the extent of particle dissolution in solution is limited by the silica limit of
22
23 solubility, the conditions of degradation within intracellular compartments can be
24
25 compared to that of an open reactor, although previous reports evidenced that the
26
27 exocytosis extent was dependent on the amount of silica in the medium.⁵⁹ This can
28
29 explain the difference evidenced for PNSPs in DMEM and within NHDFs. In the culture
30
31 medium, a decrease in initial particle size is observed after 1 week and smaller particles
32
33 are clearly visible at their vicinity (**Figure 9**). This suggests that the outer PEI/silica
34
35 layers first dissolve but, because PEI is known to promote silica precipitation,⁶⁰ the
36
37 released soluble silica species and the polyelectrolyte chains can react together to form
38
39 these new particles, as previously suggested.³⁵ In a second stage, the largest particles turn
40
41 porous, indicating that further dissolution occurs and feeds the growth of the external
42
43 smaller particles. Noticeably, within the cells, these additional particles are hardly
44
45 distinguished although the transformation from plain to porous large particles is also
46
47 observed. This result nicely correlates with our observation that, whereas BSNPs and
48
49
50
51
52
53
54
55
56
57
58
59
60

1
2
3
4 HSNPS are almost exclusively released in soluble forms during the second week, almost
5
6 30 % of PNSPs are externalized in a colloidal form that may correspond to the
7
8 newly-formed silica nanoparticles that are small enough to be expelled.
9
10

11 12 13 14 15 **CONCLUSION**

16
17 By following the evolution of silica nanoparticles with different internal nanostructures in
18
19 solution and within normal human dermal fibroblasts, we show that their degradation
20
21 pathways are very similar in all conditions although the precise composition of the
22
23 medium can impact on the kinetics of the degradation. This supports previous
24
25 assumptions that within such cells silica nanoparticles undergo a hydrolytic degradation
26
27 process, related to silica chemistry, and not a biodegradation route, that would involve a
28
29 specific biological activity. From a more fundamental point of view, these data contribute
30
31 to the on-going debate on the role of silicon and its associated biochemical pathways in
32
33 mammalian cells, that have a great importance to understand and predict the *in vivo* fate
34
35 of silica biomaterials. From a practical perspective, this implies that the intracellular fate
36
37 of silica-based nanomaterials can be controlled and predicted on the basis of
38
39 physico-chemical considerations unless they incorporate bio-responsive functions.
40
41
42
43
44
45
46
47
48
49
50
51

52 **ASSOCIATED CONTENT**

53
54
55
56
57
58
59
60

1
2
3
4 **Supporting Information.** Particle size distribution of particles in water (**Figure S1**),
5
6 DLS and zeta-metry characterization of particles during surface modification (**Table S1**),
7
8 N₂-sorption data for HSMPs (**Figure S2**), evolution of zeta potential with pH (**Figure**
9
10 **S3**), fluorescence spectra of nanoparticles (**Figure S4**), additional TEM data for
11
12 nanoparticles in culture medium (**Figures S5, S6**), addition fluorescence (**Figures S7,S9**)
13
14 and TEM images (**Figure S8**) of NHDF after contact with nanoparticles. This material is
15
16 available free of charge via the Internet at <http://pubs.acs.org>.
17
18
19
20
21
22
23
24

25 **AUTHOR INFORMATION**

26
27
28 **Corresponding Author. *Email: thibaud.coradin@upmc.fr**
29
30
31
32

33 **ACKNOWLEDGMENTS**

34
35
36 Y.S. PhD grant was funded by the China Scholarship Council. The authors thank C.
37
38 Aimé (LCMCP) for fruitful discussions and C. Illoul, and G. Mosser (LCMCP) for
39
40 technical assistance.
41
42
43
44
45
46
47
48
49
50
51
52
53
54
55
56
57
58
59
60

1
2
3
4
5
6
7
8
9
10
11
12
13
14
15
16
17
18
19
20
21
22 **REFERENCES**
23

24 (1) Slowing, I. I.; Vivero-Escoto, J. L.; Wu, C. W.; Lin, V. S. Y. Mesoporous silica
25 nanoparticles as controlled release drug delivery and gene transfection carriers. *Adv. Drug*
26 *Deliv. Rev.* **2008**, *60*, 1278-1288.

31
32 (2) Homan K. A.; Souza, M.; Truby, R.; Luke, G. P.; Green, C.; Vreeland, E.;
33 Emelianov, S. Silver nanoplate contrast agents for *in vivo* molecular photoacoustic
34 imaging. *ACS Nano* **2012**, *6*, 641-650.

35
36 (3) Yang, K.; Feng, L. Z.; Hong, H.; Cai, W. B.; Liu, Z. Preparation and
37 functionalization of graphene nanocomposites for biomedical applications. *Nature Protoc.*
38 **2013**, *8*, 2392-2403.

39
40 (4) Li, Z.; Wang, C.; Cheng, L.; Gong, H.; Yin, S.; Gong, Q.; Li Y.; Liu, Z.
41 PEG-functionalized iron oxide nanoclusters loaded with chlorin e6 for targeted, NIR light
42 induced, photodynamic therapy. *Biomaterials* **2013**, *34*, 9160-9170.
43
44
45
46
47
48
49
50
51
52
53
54
55
56
57
58
59
60

- 1
2
3
4 (5) Yao, H. J.; Zhang, Y. G.; Sun L.; Liu, Y. The effect of hyaluronic acid functionalized
5
6 carbon nanotubes loaded with salinomycin on gastric cancer stem cells. *Biomaterials* **2014**,
7
8 35, 9208-9223.
9
10
11 (6) Jeong, Y. S.; Oh, W. K.; Kim S.; Jang, J. Cellular uptake, cytotoxicity, and ROS
12
13 generation with silica/conducting polymer core/shell nanospheres. *Biomaterials* **2011**, 32,
14
15 7217-7225.
16
17
18 (7) Elgrabli, D.; Dachraoui, W.; de Marmier, H.; Menard-Moyon, C.; Begin, D.;
19
20 Begin-Colin, S.; Bianco, A.; Alloyeau, D.; Gazeau, F. Intracellular degradation of
21
22 functionalized carbon nanotube/iron oxide hybrids is modulated by iron via Nrf2 pathway.
23
24
25
26 *Sci. Rep.* **2017**, 7, 40075.
27
28
29 (8) Coradeghini, R.; Gioria, S.; Garcia, C. P.; Nativo, P.; Franchini, F.; Gilliland, D.;
30
31 Ponti J.; Rossi, F. Size-dependent toxicity and cell interaction mechanisms of gold
32
33 nanoparticles on mouse fibroblasts. *Toxicol. Lett.* **2013**, 217, 205-216.
34
35
36 (9) Hyde, E. D. E. R.; Seyfaee, A.; Neville, F.; Moreno-Atanasio, R. Colloidal Silica
37
38 Particle Synthesis and Future Industrial Manufacturing Pathways: A Review. *Ind. Eng.*
39
40
41
42 *Chem. Res.* **2016**, 55, 8891–8913.
43
44
45 (10) Li, Z. X.; Barnes, J. C.; Bosoy, A.; Stoddart, J. F.; Zink, J. I. Mesoporous silica
46
47 nanoparticles in biomedical applications. *Chem. Soc. Rev.* **2012**, 41, 2590-2605.
48
49
50 (11) Chung, T. H.; Wu, S. H.; Yao, M.; Lu, C. W.; Lin, Y. S.; Hung, Y.; Mou, C. Y.;
51
52
53
54
55
56
57
58
59
60

1
2
3
4 function of mesoporous silica nanoparticles in 3T3-L1 cells and human mesenchymal stem
5
6 cells. *Biomaterials* **2007**, *28*, 2959-2966.

7
8
9 (12) Chen, Y.; Chen, H. R.; Guo, L. M.; He, Q. J.; Chen, F.; Zhou, J.; Feng, J. W.; Shi, J.
10
11 L. Hollow/rattle-type mesoporous nanostructures by a structural difference-based selective
12
13 etching strategy. *ACS Nano* **2010**, *4*, 529-539.

14
15
16 (13) Wang Y.; Gu, H. C. Core-shell-type magnetic mesoporous silica nanocomposites for
17
18 bioimaging and therapeutic agent delivery. *Adv. Mater.* **2015**, *27*, 576-585.

19
20
21 (14) Sun, Q.; You, Q.; Pang, X. J.; Tan, X. X.; Wang, J. P.; Liu, L.; Guo, F.; Tan, F. P.; Li,
22
23 N. A photoresponsive and rod-shape nanocarrier: Single wavelength of light triggered
24
25 photothermal and photodynamic therapy based on AuNRs-capped & Ce6-doped
26
27 mesoporous silica nanorods. *Biomaterials* **2017**, *122*, 188-200.

28
29
30 (15) Liu, T. L.; Li, L. L.; Teng, X.; Huang, X. L.; Liu, H. Y.; Chen, D.; Ren, J.; He, J. Q.;
31
32 Tang, F. Q. Single and repeated dose toxicity of mesoporous hollow silica nanoparticles in
33
34 intravenously exposed mice. *Biomaterials* **2011**, *32*, 1657-1668.

35
36
37 (16) Suma, T.; Miyata, K.; Anraku, Y.; Watanabe, S.; Christie, R. J.; Takemoto, H.;
38
39 Shioyama, M.; Gouda, N.; Ishii, T.; Nishiyama, N.; Kataoka, K. Smart multilayered
40
41 assembly for biocompatible siRNA delivery featuring dissolvable silica,
42
43 endosome-disrupting polycation, and detachable PEG. *ACS Nano* **2012**, *6*, 6693-6705.

44
45
46 (17) Huang, X. L.; Teng, X.; Chen, D.; Tang, F. Q.; He, J. Q. The effect of the shape of
47
48 mesoporous silica nanoparticles on cellular uptake and cell function. *Biomaterials* **2010**,
49
50
51
52
53
54
55
56
57
58
59
60
31, 438-448.

1
2
3
4 (18) Rosenholm, J. M.; Peuhu, E.; Eriksson, J. E.; Sahlgren, C.; Lindén, M. Targeted
5 intracellular delivery of hydrophobic agents using mesoporous hybrid silica nanoparticles
6 as carrier systems. *Nano Lett.* **2009**, *9*, 3308-3311.

7
8
9
10
11 (19) Kim, M. H.; Na, H. K.; Kim, Y. K.; Ryoo, S. R.; Cho, H. S.; Lee, K. E.; Jeon, H.;
12 Ryoo, R.; Min, D. H. Facile synthesis of monodispersed mesoporous silica nanoparticles
13 with ultralarge pores and their application in gene delivery. *ACS Nano* **2011**, *5*,
14 3568-3576.

15
16
17 (20) Ratcliffe, S.; Jugdaohsingh, R.; Vivancos, J.; Marron, A.; Deshmukh, R.; Ma, J. F.;
18 Mitani-Ueno, N.; Robertson, J.; Wills, J.; Boekschoten, M. V.; Müller, M.; Mawhinney,
19 R. C.; Kinrade, S. D.; Isenring, P.; Bélanger, R. R.; Powell, J. J. Identification of a
20 mammalian silicon transporter. *Am. J. Physiol. Cell Physiol.* **2017**, *312*, C550-C561.

21
22 (21) Croissant, J. G.; Fatieiev, Y.; Kashab, N. M. Functional Nanoparticles: Degradability
23 and Clearance of Silicon, Organosilica, Silsesquioxane, Silica Mixed Oxide, and
24 Mesoporous Silica Nanoparticles. *Adv. Mater.* **2017**, *29*, 1604634

25
26
27 (22) Braun, K.; Pochert, A.; Beck, M.; Fiedler, R.; Gruber, J.; Lindén, M. Dissolution
28 kinetics of mesoporous silica nanoparticles in different simulated body fluids. *J. Sol-Gel*
29 *Sci. Technol.* **2016**, *79*, 319-327.

30
31
32 (23) Yang, Y.; Coradin, T. A green route to silica nanoparticles with tuneable size and
33 structure. *Green Chem.* **2008**, *10*, 183-190.

1
2
3
4 (24) Quignard, S.; Masse, S.; Laurent, G.; Coradin, T. Introduction of disulfide bridges
5
6 within silica nanoparticles to control their intra-cellular degradation. *Chem. Commun.* **2013**,
7
8 *49*, 3410-3412.

9
10
11 (25) Corsi, F.; De Palma, C.; Colombo, M.; Allevi, R.; Nebuloni, M.; Ronchi, S.; Rizzi,
12
13 G.; Tosoni, A.; Trabucchi, E.; Clementi, E.; Prospero, D. Towards Ideal
14
15 Magnetofluorescent Nanoparticles for Bimodal Detection of Breast-Cancer Cells. *Small*
16
17 **2009**, *5*, 2555-2564.

18
19
20 (26) Dove, P. M.; Han, N.; Wallace, A. F.; De Yoreo, J. J. Kinetics of amorphous silica
21
22 dissolution and the paradox of silica polymorphs. *Proc. Natl. Acad. Sci. USA* **2008**, *105*,
23
24 9903-9908.

25
26
27 (27) Iler, R. K. *The Chemistry of Silica: Solubility, Polymerization, Colloid and Surfaces*
28
29 *Properties, and Biochemistry*; Wiley: New York, 1979.

30
31
32 (28) Ehrlich, H.; Demadis, K. D.; Pokrovsky, O. S.; Koutsoukos, P. G. Modern Views on
33
34 Desilicification: Biosilica and Abiotic Silica Dissolution in Natural and Artificial
35
36 Environments. *Chem. Rev.* **2000**, *110*, 4656-4689.

37
38
39 (29) Viitala, R.; Jokinen, M.; Tuusa, S.; Rosenholm, J. B.; Jalonen, H. Adjustably
40
41 bioresorbable sol-gel derived SiO₂ matrices for release of large biologically active
42
43 molecules. *J. Sol-Gel Sci. Technol.* **2005**, *36*, 147-156.

44
45
46 (30) Finnie, K. S.; Waller, D. J.; Perret, F. L.; Krause-Heuer, A. M.; Lin, H. Q.; Hanna, J.
47
48 V.; Barbé, C. J. Biodegradability of sol-gel silica microparticles for drug delivery. *J.*
49
50 *Sol-Gel Sci. Technol.* **2009**, *49*, 12-18.

- 1
2
3
4 (31) Yamada, H.; Urata, C.; Aoyama, Y.; Osada, S.; Yamauchi, Y.; Kuroda, K. Preparation
5
6 of Colloidal Mesoporous Silica Nanoparticles with Different Diameters and Their Unique
7
8 Degradation Behavior in Static Aqueous Systems. *Chem. Mater.* **2012**, *24*, 1462-1471.
9
10
11 (32) Bass, J. D.; Grosso, D.; Boissière, C.; Belamie, E.; Coradin, T.; Sanchez, C. Stability
12
13 of Mesoporous Oxide and Mixed Metal Oxide Materials in Biologically Relevant
14
15 Conditions. *Chem. Mater.* **2007**, *19*, 4349-4356.
16
17
18 (33) Galarneau, A.; Nader, M.; Guenneau, F.; Di Renzo, F.; Gedeon, A. Understanding
19
20 the Stability in Water of Mesoporous SBA-15 and MCM-41. *J. Phys. Chem. C* **2007**, *111*,
21
22 8268-8277.
23
24
25 (34) He, Q. J.; Shi, J. L.; Zhu, M.; Chen, Y.; Chen, F. The three-stage *in vitro* degradation
26
27 behavior of mesoporous silica in simulated body fluid. *Microp. Mesop. Mater.* **2010**, *131*,
28
29 314-320.
30
31
32 (35) Chen, K.; Zhang, J.; Gu, H. Dissolution from inside: a unique degradation behaviour of
33
34 core-shell magnetic mesoporous silica nanoparticles and the effect of polyethyleneimine
35
36 coating. *J. Mater. Chem.* **2012**, *22*, 22005-22012.
37
38
39 (36) Boissière, M.; Meadows, P. J.; Brayner, R.; Hélarý, C.; Livage, J.; Coradin, T.
40
41 Turning biopolymer particles into hybrid capsules: the example of silica/alginate
42
43 nanocomposites. *J. Mater. Chem.* **2006**, *16*, 1178-1182.
44
45
46 (37) Allouche, J.; Boissière, M.; Hélarý, C.; Livage, J.; Coradin, T. Biomimetic core-shell
47
48 gelatine/silica nanoparticles: a new example of biopolymer-based nanocomposites. *J. Mater.*
49
50
51
52
53
54
55
56
57
58
59
60

- 1
2
3
4 (38) Slowing I. I.; Vivero-Escoto, J. L.; Zhao, Y.; Kandel, K.; Peeraphatdit, C.; Trewyn,
5
6 B. G.; Lin, V.S. Exocytosis of mesoporous silica nanoparticles from mammalian cells:
7
8 from asymmetric cell-to-cell transfer to protein harvesting. *Small* **2011**, *7*, 1526-1532.
9
10
11 (39) Quignard, S.; Mosser, G.; Boissière, M.; Coradin, T. Long-term fate of silica
12
13 nanoparticles interacting with human dermal fibroblasts. *Biomaterials* **2012**, *33*,
14
15 4431-4442.
16
17
18 (40) Zhai, W.; He, C.; Wu, L.; Zhou, Y.; Chen, H.; Chang, J.; Zhang, H. Degradation of
19
20 hollow mesoporous silica nanoparticles in human umbilical vein endothelial cells. *J.*
21
22 *Biomed. Mater. Res. B* **2012**, *100B*, 1397-1403.
23
24
25 (41) Chen, G.; Teng, Z.; Su, X.; Liu, Y.; Lu, G. Unique Biological Degradation Behavior
26
27 of Stöber Mesoporous Silica Nanoparticles from Their Interiors to Their Exteriors. *J.*
28
29 *Biomed. Nanotechnol.* **2015**, *11*, 722-729.
30
31
32 (42) Kempen, P. J.; Greasley, S.; Parker, K. A.; Campbell, J. L.; Chang, H.-Y.; Jones, J.
33
34 R.; Sinclair, R.; Gambhir, S. S.; Jokerst, J. V. Theranostic Mesoporous Silica
35
36 Nanoparticles Biodegrade after Pro-Survival Drug Delivery and Ultrasound/Magnetic
37
38 Resonance Imaging of Stem Cells. *Theranostics* **2015**, *5*, 631-642.
39
40
41 (43) Bergman, L.; Kankaanpää, P.; Tiitta, S.; Duchanoy, A.; Ji, L.; Heino, J.; Lindén, M.
42
43 Intracellular Degradation of Multilabeled Poly(Ethylene imine)-Mesoporous Silica-Silica
44
45 Nanoparticles: Implications for Drug Release. *Mol. Pharm.* **2013**, *10*, 1795-1803
46
47
48
49
50
51
52
53
54
55
56
57
58
59
60

- 1
2
3
4 (44) Couleaud, P.; Morosini, V.; Frochot, C.; Richeter, S.; Raehm, L.; Durand, J. O.
5
6 Silica-based nanoparticles for photodynamic therapy applications. *Nanoscale* **2010**, *2*,
7
8 1083-1095.
9
10
11 (45) Montalti, M.; Prodi, L.; Rampazzo, E.; Zaccheroni, N. Dye-doped silica nanoparticles
12
13 as luminescent organized systems for nanomedicine. *Chem. Soc. Rev.* **2014**, *43*, 4243-4268.
14
15
16 (46) Li, Z.; Yuan, D.; Jin, G.; Tan, B.; He, C. Facile Layer-by-Layer Self-Assembly
17
18 toward Enantiomeric Poly(lactide) Stereocomplex Coated Magnetite Nanocarrier for
19
20 Highly Tunable Drug Deliveries. *ACS Appl. Mater. Interfaces* **2016**, *8*, 1842-1853.
21
22 (47)
23 Mebert, A. M.; Aimé, C.; Alvarez, G. S.; Shi, Y.; Flor, S. A.; Lucangioli, S. E.;
24
25 Desimone, M. F.; Coradin, T. Silica core-shell particles for the dual delivery of gentamicin
26
27 and rifamycin antibiotics. *J. Mater. Chem. B* **2016**, *4*, 3135-3144.
28
29
30
31
32 (48) Andersson, J.; Rosenholm, J.; Areva, S.; Lindén, M. Influences of Material
33
34 Characteristics on Ibuprofen Drug Loading and Release Profiles from Ordered Micro- and
35
36 Mesoporous Silica Matrices. *Chem. Mater.* **2004**, *16*, 4160-4167
37
38
39
40 (49) Bouledjoudja, A.; Masmoudi, Y.; Van Speybroeck, M.; Schueller, L. Badens, E.
41
42 Impregnation of Fenofibrate on mesoporous silica using supercritical carbon dioxide. *Int. J.*
43
44 *Pharm.* **2016**, *499*, 1-9.
45
46
47
48 (50) Zhou, Z.; Zhang, C.; Qian, Q.; Ma, J.; Huang, P.; Zhang, X.; Pan, L.; Gao, G.; Fu, H.;
49
50 Fu, S.; Song, H.; Zhi, X.; Ni, J.; Cui, D. Folic acid-conjugated silica capped gold
51
52 nanoclusters for targeted fluorescence/X-ray computed tomography imaging. *J.*
53
54 *Nanobiotechnol.* **2013**, *11*, 17.
55
56
57

- 1
2
3
4 (51) Nakamura, T.; Sugihara, F.; Matsushita, H.; Yoshioka, Y.; Mizukami, S.; Kikuchi, K.
5
6 Mesoporous silica nanoparticles for ^{19}F magnetic resonance imaging, fluorescence imaging,
7
8 and drug delivery. *Chem. Sci.* **2015**, *6*, 1986-1990.
9
10
11 (52) van Blaaderen, A.; Vrij, A. Synthesis and characterization of colloidal dispersions of
12
13 fluorescent, monodisperse silica spheres. *Langmuir* **1992**, *8*, 2921-2931.
14
15
16 (53) Chen, F.; Hong, H.; Shi, S. X.; Goel, S.; Valdovinos, H. F.; Hernandez, R.; Theuer,
17
18 C. P.; Barnhart, T. E.; Cai, W. B. Engineering of Hollow Mesoporous Silica Nanoparticles
19
20 for Remarkably Enhanced Tumor Active Targeting Efficacy. *Sci. Rep.* **2014**, *4*, 5080.
21
22
23 (54) Wang, X.; Masse, S.; Laurent, G.; H elary, C.; Coradin, T. Impact of
24
25 Polyethylenimine Conjugation Mode on the Cell Transfection Efficiency of Silica
26
27 Nanovectors. *Langmuir* **2015**, *31*, 11078-11085.
28
29
30 (55) Drescher, D.; Orts-Gil, G.; Laube, G.; Natte, K.; Veh, R. W.;  osterle, W.; Kniepp, J.
31
32 Toxicity of amorphous silica nanoparticles on eukaryotic cell model is determined by
33
34 particle agglomeration and serum protein adsorption effects. *Anal. Bioanal. Chem.* **2011**,
35
36 *400*, 1367-1373
37
38
39 (56) Noble, J. E.; Wang, L.; Cole, K. D.; Gaigalas, A. K. The effect of overhanging
40
41 nucleotides on fluorescence properties of hybridising oligonucleotides labelled with
42
43 Alexa-488 and FAM fluorophores. *Biophys. Chem.* **2005**, *113*, 255-263.
44
45
46
47
48
49
50
51
52
53
54
55
56
57
58
59
60

1
2
3
4 (57) Soulé, S.; Bulteau, A. L.; Faucher, S.; Haye, B.; Aimé, C.; Allouche, J.; Dupin, J. C.;
5
6 Lespes, G.; Coradin, T.; Martinez, H. Design and Cellular Fate of Bioinspired Au-Ag
7
8 Nanoshells@hybrid Silica Nanoparticles. *Langmuir* **2016**, *32*, 10073-10082.

9
10
11 (58) Tappel, A. L.; Shibko, S.; Stein, M.; Susz, J. P. Studies on the Composition of
12
13 Lysosomes. *J. Food. Sci.* **1965**, *30*, 498-503.

14
15
16 (59) Chu, Z.; Huang, Y.; Tao, Q.; Li, Q. Cellular uptake, evolution, and excretion of silica
17
18 nanoparticles in human cells. *Nanoscale* **2011**, *3*, 3291-3299.

19
20
21 (60) Demadis, K. D.; Pachis, K.; Ketsetzi, A.; Stathoulopoulou, A. Bioinspired control of
22
23 colloidal silica in vitro by dual polymeric assemblies of zwitterionic phosphomethylated
24
25 chitosan and polycations or polyanions. *Adv. Colloid Interface Sci.* **2009**, *151*, 33-48.
26
27
28
29
30
31
32
33
34
35
36
37
38
39
40
41
42
43
44
45
46
47
48
49
50
51
52
53
54
55
56
57
58
59
60

TOC graphics

